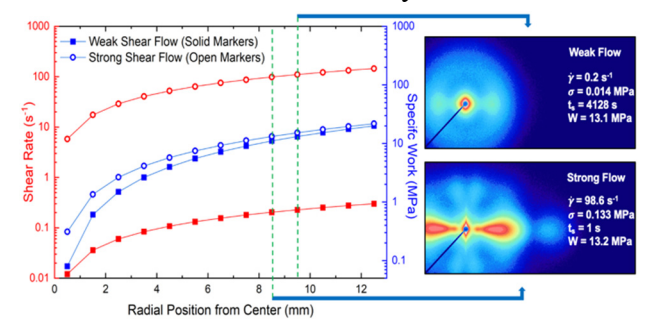
Particle Concentration Promotes Flow-Induced Crystallization of High Molecular Weight Isotactic Polypropylene

Benson J. Jacob¹, Xiaoshi Zhang³, Jongkyeong Kim², Jason D. Alexander¹, Manoela E. Cangussú⁴, Alicyn M. Rhoades³, and Ralph H. Colby²

For Table of Contents use only:



ABSTRACT: Intervals of shear flow stretch polymer chains and form flow-induced precursors, which accelerate crystallization and transform the crystalline morphology from isotropic spherulites to anisotropic structures. The flow-induced crystallization of two commercial samples of isotactic polypropylene with nearly identical molecular weight distributions, differing in concentrations of catalyst residue particles, was investigated using dynamic rheology and *ex situ* Synchrotron X-ray scattering. Upon the application of flow, the sample with higher particle concentration crystallized at faster rates relative to the sample with lower levels of heterogenous impurities. The nucleation ability of these particles was particularly pronounced at lower levels of deformation, while flow effects became prominent as larger deformations were applied. For sufficiently strong flows ($\dot{\gamma} \leq 145 \text{ s}^{-1}$), a lower critical shear stress (~0.096 MPa) was observed for the formation of shish-kebab structures in the sample with higher concentrations of particles.

¹Department of Chemical Engineering, The Pennsylvania State University, University Park, Pennsylvania 16802, United States

²Department of Materials Science and Engineering, The Pennsylvania State University, University Park, Pennsylvania 16802, United States

³School of Engineering, Penn State Behrend, Erie, Pennsylvania 16563, United States

⁴Braskem Innovation and Technology Center, Via Oeste, Lote 5, Passo Raso, Triunfo, 95853, RS, Brazil

In this work, we have also identified the formation of shish-kebab structures in the presence of weak flow ($\dot{\gamma} \leq 0.3 \text{ s}^{-1}$) when sheared for long durations of time. For equivalent levels of specific work within both flow regimes, the morphologies of these anisotropic structures were found to be characteristically distinct from one another. The long period and degree of crystallinity were also found to increase with shear stress above the stress level needed for the formation of shish-kebab structures.

INTRODUCTION

Polypropylene is one of the most widely used synthetic polymers in the world. When semicrystalline polymer melts are subject to large deformations prior to supercooling, flow-induced precursors can form, resulting in an increased number density of nuclei and a change in crystalline morphology. This phenomenon is referred to as flow-induced crystallization (FIC) and is ubiquitous in polymer melt processing, such as injection molding or film blowing. These flow fields contribute to changes in the crystalline microstructure and are associated with increased tensile strength relative to quiescent crystallization. 10,11

Polymer crystallization is a chain ordering process consisting of nuclei formation and subsequent crystal growth.^{12–14} The nucleation process can be altered in the presence of particles or with the application of flow. Nuclei may be formed in the melt itself through homogenous nucleation, or heterogeneously at an interface. For isotactic polypropylene heterogenous nucleation occurs more readily at elevated temperatures (60-150°C), while homogenous nucleation becomes much more significant at lower temperatures (<60°C).^{15,16} It has been suggested that particles can act as heterogeneous nucleation sites that lower the surface free energy barrier with respect to the nucleus.^{15,17,18} Epitaxial nucleation has also been thought to explain the nucleating

ability of particles, where a certain degree of lattice matching between the crystal lattices of the polymer and the particles has been suggested to be necessary for nucleation. 19,20

In flow, coiled polymer chains align and stretch, which lowers the melt entropy and decreases the nucleation barrier, allowing for an increased concentration of nuclei upon crystallization. This results in faster crystallization kinetics, 3,5,7,18,21,22 elevated crystallization temperatures, 23–25 and a transformation in the crystalline structure from larger isotropic spherulites to much smaller spherulites, and eventually to anisotropic morphologies for isotactic polypropylene. 24,26–29

Of these anisotropic structures, highly oriented shish-kebabs are one of the most distinctive morphologies. At high stress levels, deformations first promote close lateral packing of dense chain extended fibrillar structures known as shish. 25-27,29-31 Thereafter, lamellae grow transversally outward upon crystallization to form kebab structures. Hsiao et al. observed the structure formation of these shish-kebabs using *in situ* X-ray scattering with a shear stage. 26,29,32 They sheared isotactic polypropylene at 155 and 165°C at a shear rate of 60 s⁻¹ for 5 seconds and first observed scattering intensities parallel to the flow direction, signifying the formation of shish. A short time later the lamellae (kebabs) grew perpendicular to the shish, as indicated by a change in the anisotropic scattering profile. Using a pressure driven flow, Balzano et al. 27 were able to induce shish-kebab structures at high shear stresses. Upon reaching a critical shear stress of ~0.14 MPa, the spherulites were transformed to highly birefringent structures orienting along the flow direction.

In typical experiments performed by Peters^{27,31,33} and Kornfield^{5,21,34} groups, a Poiseuille flow geometry is used to apply intense shear at temperatures close to ~145 °C. In these geometries, the shear stress is largest at the walls and decreases to zero at the center of the geometry. This results in a "skin-core" morphology where a highly anisotropic layer is formed closest to the walls, followed by a fine-grain layer, and an isotropic spherulitic core, which are observed using in-situ

X-ray scattering or optical microscopy. To form these anisotropic shear layers, it is thought that the shear stress must exceed a certain threshold, while the deformation also needs to be sufficiently high.^{25,27}

The longest chains in a polymer melt play a critical role in flow-induced crystallization. Several studies have reported that these high molecular weight chains are most influential in generating FIC effects, as opposed to flow acting equally amongst all chains in a given molecular weight distribution. 3,18,22,32 Somani et al. 32 used *in-situ* small-and-wide angle X-ray scattering to investigate the role of high molecular weight species on the crystallization of isotactic polypropylene under shear flow. They compared two samples of isotactic polypropylene with the same number-average molecular weights with differing high molecular weight tails, and found that the sample with the higher molecular weight tail formed shish structures earlier, and exhibited faster crystallization kinetics. These long chains are the slowest to relax and are the easiest to be stretched and oriented by flow, which are essential to forming flow-induced precursors. 4,18,25 To stretch these long chains, the shear rate must exceed the reciprocal of their relaxation (Rouse) time, such that $\dot{\gamma}\tau_R \geq 1$. 24,25,30,35,36

Specific work is an important process parameter that controls the strength of flow-induced crystallization for low levels of deformation. This is the energy per unit volume and is expressed as stress σ times strain γ :

$$W = \sigma \gamma = \eta \dot{\gamma}^2 t_s \tag{1}$$

where η is the steady state shear viscosity at a constant shear rate $\dot{\gamma}$, and t_s is the duration of shear applied to the sample. With increasing levels of specific work, more chains can aggregate and form stable nuclei. Even low levels of specific work have been shown to accelerate the rate of crystallization, while the formation of anisotropic structures only occurs after sufficient levels of

specific work are applied. At low levels of deformation, Hamad et al.²⁴ observed the formation of rice grain morphologies using Atomic Force Microscopy of sheared samples of isotactic polypropylene. These structures were randomly oriented, ranging in lengths of 1.5 – 3.0 micrometers, depending on the level of specific work. Ryan et al.^{4,41} had also identified a critical work threshold for polyethylene, where at this critical value the morphology transformed from being unoriented to forming structures oriented along the flow direction.

Catalyst residues have been an issue related to polyolefin polymerization since the advent of the Phillips catalyst. While great efforts have been made to reduce these residues, trace levels still persist after polymerization. However, very little work has been performed to determine the magnitude to which these particulate impurities affect the flow-induced crystallization of neat materials.

In this work, we investigate the flow-induced crystallization of two commercial samples of polypropylene that have nearly identical rheological properties and high molecular weight tails, but differ in concentrations of catalyst residue particles from polymerization. We use a rotational rheometer to apply controlled deformations and monitor crystallization dynamically in the melt to explore the flow-induced nucleation kinetics and linear viscoelastic crystallization temperatures. The structural morphology and changes in crystalline microstructure are revealed through small-and-wide angle X-ray scattering. It was found that higher particle concentrations promoted flow-induced crystallization effects, which resulted in faster flow-induced nucleation kinetics, and a slightly lower critical shear stress for the formation of anisotropic shish-kebab structures.

EXPERIMENTAL

Materials. Two commercial samples of isotactic polypropylene (denoted iPP6 and iPP7) were provided by Phillips 66. The samples were produced in a slurry polymerization process using a Ziegler-Natta catalyst. The concentration of catalyst residue of iPP6 and iPP7 are 166 and 48 ppm, respectively, as provided by the manufacturer. These samples were chosen to compare the effect of particle concentration on the flow-induced crystallization of samples with *nearly identical* rheological properties and high molecular weight tails. Material and linear viscoelastic properties can be seen in Table 1.

Table 1. Material and Linear Viscoelastic Properties of iPP6 and iPP7

Tuble 1. Muceliul und Eliteur Viscoelustie Troperties of it to und it t		
	iPP6	iPP7
Mw [kg/mol]	833	820
M _n [kg/mol]	73	79
M _{max} [kg/mol]	7000	7000
XS [%] ^a	3.6	3.7
η ₀ [kPa s] ^b	170*	170
m ^b	0.7*	0.7
τ [s] ^b	10*	10
τ _{term} [s] ^c	0.59*	0.59

^aXylene-soluble fraction, indicative of atactic content (ASTM D5492).

^bThe zero-shear viscosity, η_0 , relaxation time, τ , and shear thinning exponent, m, were estimated from the fit of the flow curves to the Cross Model (Eq. 2).

^cThe terminal relaxation time estimated from the inverse of the frequency at the dynamic moduli crossover.

^{*}Rheological values taken from ref,⁴² where iPP7 coincides with iPP6 (see Figure 2).

Gel Permeation Chromatography. A high temperature GPC (Polymer Char GPC IR5) equipped with infrared detector IR5 and an eight-angle light scattering detector (from Wyatt) was used in this study. GPC separation was carried out by using three columns Tosoh 30 μm mixed bed at 160°C, flow rate of 1 mL/min and injection volume of 200 μL. Polymer samples were dissolved in trichlorobenzene (TCB) at a concentration of 1mg/mL. To ensure the complete dissolution, samples were kept at 160°C for 90 minutes. TCB was used as the mobile phase. Reported values are the average of several replicates.

The long chain branching determination can be obtained through GPC by the combination of a concentration sensitive detector and a molar mass sensitive detector. The long chain branching (LCB) detection is based on the reduction of viscosity and radius of gyration of a polymer chain with LCB when compared with a linear reference with same chemical composition and molar mass distribution. The difference in the slope of the Mark-Houwink plot (Log IV x Log M) and conformation plot (Log R_g x Log M) between linear and branched samples is directly related to the amount of LCB, as an effect of the more compact form assumed by the branched chains. 43–48

Linear Viscoelasticity. All rheological measurements were carried out using a strain-controlled ARES G2 rotational rheometer (TA Instruments, New Castle, DE), and run under nitrogen to minimize sample oxidation. The linear viscoelastic responses of the two materials were determined using a 25 mm parallel plate geometry at 170 °C with frequencies ranging from 0.001 to 100 rad/sec. A strain amplitude of 0.05 was used, while at low frequencies, strain amplitudes were increased to provide sufficient torque to maintain measurable stress levels, while still remaining in the linear viscoelastic regime.

Flow-Induced Crystallization. To investigate flow-induced crystallization, a rotational rheometer equipped with 8 mm cone (0.1 rad cone angle and 0.046 mm truncation gap) and plate

fixtures was used to apply intervals of shear at 170 °C and monitor crystallization using both isothermal oscillatory time sweeps and non-isothermal temperature ramps at frequency of 0.5 rad/sec, with a stain amplitude of 0.05.

Crystallization was monitored through the samples viscoelastic response at a constant frequency, following the criteria developed by Pogodina and Winter.⁴⁹ As the sample crystallizes from the melt, the material properties transform from viscous to elastic response. In shear-induced crystallization, this is illustrated by the storage modulus (G') surpassing the loss modulus (G'') at a constant frequency, which causes a decrease in the loss tangent $tan\delta = G''(\omega_0)/G'(\omega_0)$. The crossover of the storage and loss moduli results in a value of $tan\delta = 1$, which is a convenient and reproducible measure for the linear viscoelastic crystallization time.^{7,18,38,49}

Oscillatory Time Sweep. Prior to crystallization, samples were annealed in the rheometer well above the equilibrium melting temperature $(T_m^0 = 187 \, ^{\circ}\text{C})^{50}$ at 220 $^{\circ}\text{C}$ for 5 minutes to remove previous thermal history from sample preparation. The sample was then cooled to 170 $^{\circ}\text{C}$, just above the nominal melting temperature, and sheared at a constant shear rate for various durations of time. To measure isothermal crystallization kinetics, samples were quenched to the desired crystallization temperature (cooling rate of ~10 $^{\circ}\text{C/min}$), after which an oscillatory time sweep was initiated using a constant frequency of 0.5 rad/sec and strain amplitude of 0.05.

Oscillatory Temperature Ramp. A similar protocol to that described above was used to monitor non-isothermal crystallization, with the exception of slowly cooling the sample and measuring the temperature at which the sample crystallizes (where $tan\delta = 1$). As for the oscillatory time sweep experiments, samples were annealed at 220 °C for 5 minutes, and cooled to the shearing temperature ($T_s = 170$ °C). After applying intervals of shear at 170 °C, an oscillatory

temperature ramp is initiated using a constant frequency of 0.5 rad/sec and strain amplitude of 0.05, while cooling the sample at 1 °C/min.

X-ray Scattering. Sample disks were compression molded into 25 mm disks under vacuum and annealed at 220 °C for 30 minutes to erase any prior memory that may exist from pellet extrusion. ^{18,25} The samples were sheared in a rotational rheometer using 25 mm parallel plates to achieve varying levels of shear stress at different radial positions on a single sample. Simultaneous small- and wide-angle Synchrotron X-ray scattering (SAXS/WAXS) experiments were performed at Beamline 5ID-D of the Dupont-Northwestern-Dow Collaborative Access Team Synchrotron Research Center at the Advanced Photon Source, Argonne National Laboratory. The patterns are shown as a function of the scattering wavevector, q, (q = $(4\pi/\lambda) \sin(\theta/2)$, where θ is the scattering angle and $\lambda = 0.7293$ Å), measured in the range of 0.0025–4.46 Å⁻¹. The sample to detector distances for SAXS and WAXS were 8505 mm and 200.25 mm, respectively. A beam size of 0.25 mm and an exposure time of 1 second was used per scan. SAXS and WAXS patterns were analyzed using Igor Pro (WaveMetrics, Portland, OR) with the Nika 2D SAS macros package.

RESULTS AND DISCUSSION

To determine the effects that foreign particles have on the flow-induced crystallization of neat semicrystalline polymers, two high molecular weight samples of polypropylene with nearly identical rheological properties and high molecular weight tails were investigated.

Sample Characteristics. From Table 1, we see both samples of polypropylene are very similar to one another, with the exception of the concentrations of particle impurities. These particulates are attributed to catalyst residue and catalyst support fragments stemming from a slurry polymerization process using a Ziegler-Natta catalyst, where iPP6 has roughly 3.5 times the concentration of catalyst residue compared to iPP7 (provided by the manufacturer).

Elemental analysis was performed using inductively coupled plasma mass spectroscopy (ICP-MS), where high levels of Titanium, Magnesium, Aluminum, and Silicon were found, as shown in Table 2. These impurities are presumably TiCl₄, MgO, SiO₂, and an Aluminum co-catalyst (metal-alkyl; Al(C₂H₅)₃), all of which are expected in Ziegler-Natta polymerization.^{24,51} TiCl₄ is the primary catalyst, while MgO and SiO₂ are probable catalyst support materials.

Table 2. Particle Concentrations of iPP6 and iPP7

	iPP6	iPP7
Catalyst Residue [ppm]	166	48
Ti [ppm]	2.3	0.8
Mg [ppm]	17.7	10.3
Al [ppm]	73.3	29.8
Si [ppm]	121.4	71.4

The molecular weight distributions can be seen in Figure 1, obtained through gel permeation chromatography (GPC), where no branching has been detected in either sample. The absence of long chain branching can be seen in the conformation plot, where a straight line with a slope greater than 0.5 is expected for long and linear chains⁵² as observed for both iPP6 and iPP7

(see SI; Figure S1). From the GPC curves, both samples are similar in distribution, overlapping in the low and high molecular weight regions, while iPP7 has a slightly higher fraction of shorter chains, as seen towards the middle of the distribution. Nonetheless, the high molecular weight tails are of particular importance for flow-induced crystallization. 3,25,32,53 These long polymer chains are thought to contribute most strongly towards nucleation, as these chains can most easily be stretched by flow fields. The high molecular weight tails of both iPP6 and iPP7 are nearly identical to one another. As the deformation rate increases, the minimum molecular weight for chains to be stretched decreases (see Figure 1b), and can be computed from the Rouse time such that 54,55 : $\tau_R =$ $\left(\frac{M}{M_o}\right)^2 \tau_e$ where M_e is the entanglement molecular weight and τ_e is the Rouse time of an entanglement strand. For isotactic polypropylene at 170 °C, the entanglement molecular weight $M_e \equiv \rho RT/G_e = 5.25$ kg/mol (where ρ is the density, R is the gas constant, T is the absolute temperature, and G_e is the plateau modulus), while the Rouse time for an entanglement strand $\tau_e =$ 1.5×10^{-7} s. 18,56 To better quantify these high molecular weight tails, we will also define a "maximum" molecular weight (M_{max}), which is obtained by taking the natural logarithm of the weight fraction vs linear M_w, where the slope at large M_w is defined as -1/M_{max}, i.e., $w_N \sim exp\left(\frac{-M}{M_{max}}\right)$ at large M (see Table 1 and Figure S2).²⁵ M_{max} is a simple means to characterize the exponential decay of the high molecular weight tail of the distribution.

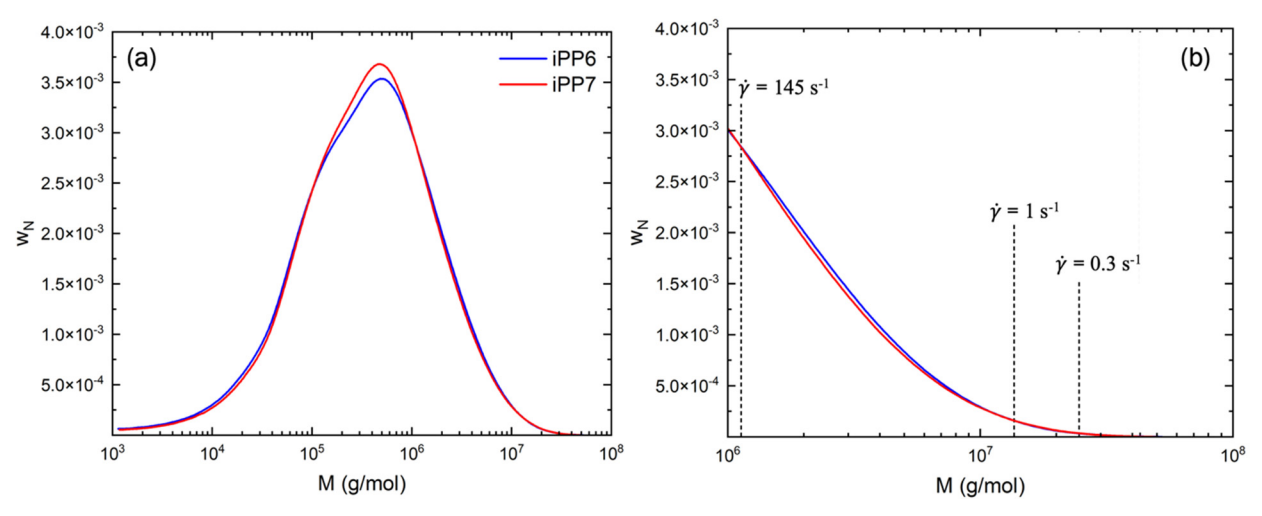


Figure 1. (a) Weight fraction molecular weight distribution of iPP6 (blue) and iPP7 (red) (b) Magnified view of high molecular weight tails. With larger shear rates, the fraction of stretchable chains increases.

Dynamic rheology is another important characterization technique for flow-induced crystallization. Figure 2a shows the linear viscoelastic response of both samples at 170 °C (above the nominal melting temperature), with frequencies spanning five decades from 10⁻³ to 100 rad/sec, where both iPP6 and iPP7 have identical viscoelastic responses. With the two samples having the same linear viscoelasticity and very similar molecular weight distributions, the relaxation times are equivalent (see Table 1). As expected, the complex viscosity (Figure 2b) of iPP6 and iPP7 are also identical to one another and demonstrate an indistinguishable shear thinning behavior, occurring even at low frequencies, owing to their high molecular weight.

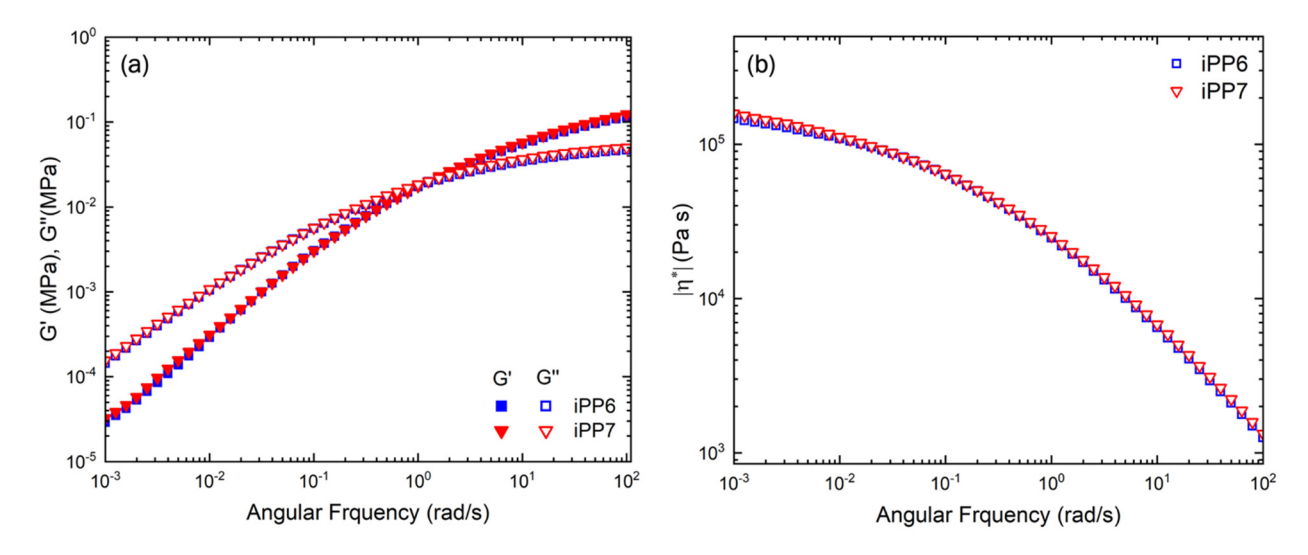


Figure 2. (a) Storage modulus (G') and loss modulus (G'') as a function of angular frequency at reference temperature of 170 °C (b) Complex viscosity as a function of angular frequency at reference temperature of 170 °C.

In a previous publication,⁴² our group extensively studied the rheological response of various entangled isotactic polypropylene melts under steady shear flows. Parisi et al. constructed flow curves spanning from the Newtonian plateau to a clear shear-thinning regime by combining various rheological techniques and instruments. These flow curves were well represented by the Cross model,⁵⁷

$$\eta(\dot{\gamma}) = \frac{\eta_0}{1 + (\dot{\gamma}\tau)^m} \tag{2}$$

where η_0 is the zero-shear viscosity, τ is the relaxation time of the chains in the distribution, $\dot{\gamma}$ is the shear rate, and m is the shear thinning exponent (listed in Table 1). It was established that the Cox-Merz rule⁵⁸ was well obeyed for these samples,⁴² as at $\omega = \dot{\gamma}$, the complex viscosity at a given frequency was equal to the steady state shear viscosity, $|\eta^*(\omega)| = \eta(\dot{\gamma})$.

Flow-Induced Crystallization. *Shear-Induced Crystallization Kinetics*. Specific work is a key parameter that governs the strength of flow-induced crystallization for low levels of deformation. ^{1,4,9,18,37} In this experiment, we make use of a shearing and quenching protocol where

samples are sheared at 170 °C (above their nominal melting point) and then quenched (at ~ 10 °C/min) to a crystallization temperature of 150 °C without undershooting (i.e. upon approaching 150 °C samples are cooled at a slightly slower rate to minimize temperature fluctuations below the desired crystallization temperature), where the time dependent linear viscoelasticity at a fixed frequency is monitored.

Figure 3 presents the linear viscoelastic crystallization kinetics of iPP6 and iPP7 for various levels of specific work at a fixed shear rate of 1 s⁻¹. The shear rate used in this experiment is above the reciprocal of the relaxation time ($\tau = 10$ s, see Table 1), where only a small fraction of chains in the high molecular weight tail of the distribution can be stretched by the flow (see Figure 1b). Both iPP6 and iPP7 have virtually identical high molecular weight tails, yet the two samples show different degrees of flow-induced crystallization. From the Rouse time, a shear rate of 1 s⁻¹ corresponds to a minimum molecular weight of 1.4 \times 10⁴ kg/mol that can be stretched by the flow. The weight fraction of stretchable chains can be obtained by integrating the molecular weight distribution at this position upward, resulting in a fraction of 0.0029 chains that are stretched by the flow for both iPP6 and iPP7 at a shear rate of 1 s⁻¹.

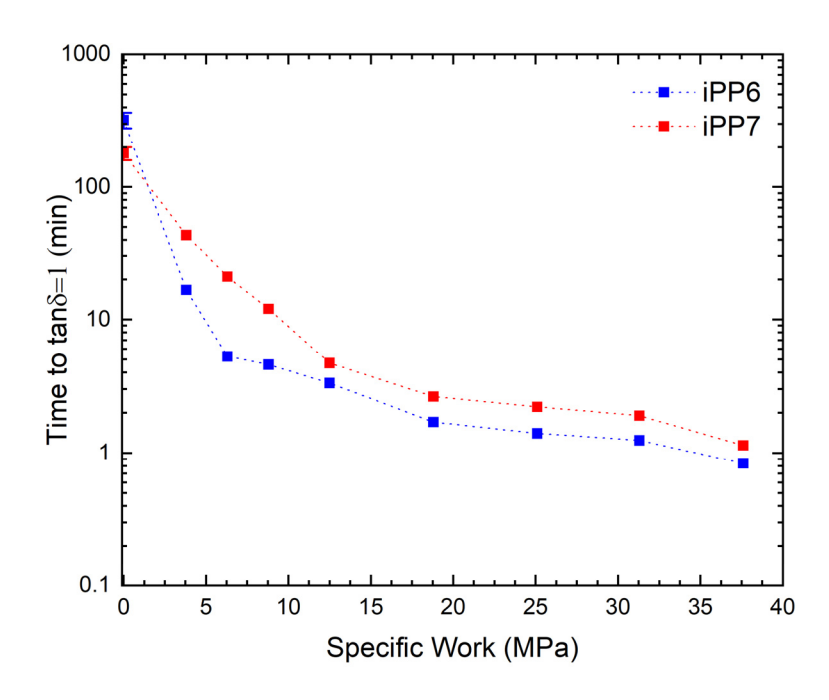


Figure 3. Crystallization time versus specific work with a shear rate of 1 s⁻¹ at a crystallization temperature of 150 °C. Upon the application of flow, iPP6, the sample with more particulates, crystallizes faster than iPP7.

When subject to flow, iPP6 exhibits more pronounced FIC kinetics than iPP7. At applied work levels less than W = 18 MPa, the crystallization times of iPP6 are appreciably faster than those of iPP7. Moreover, the initial slope of iPP6's crystallization time vs specific work in Figure 3 is notably steeper than that of iPP7, until both samples reach a saturation threshold near 18 MPa. As the applied specific work exceeds W = 18 MPa, further increases in specific work have minimal effects on the kinetics, and both samples approach comparable crystallization times with iPP6 still being ~1.5x faster. The saturation work level in Figures 3 is in agreement with results obtained by Hamad et al. for lower molecular weight samples of polypropylene. Interestingly, in the case of quiescent crystallization (W = 0 MPa in Figure 3), iPP7 crystallizes faster than iPP6 (consistent with DSC on quiescent samples, see Figure S10), which suggests that these particles are not nucleating agents. Yet, the crystallization time of iPP6 is reduced by a factor of ~335 from

quiescent crystallization to the maximum specific work applied (W = 38 MPa), while in the same range, iPP7 is only reduced by a factor of \sim 172.

Under quiescent conditions, the addition of nucleating agents such as sodium 2,20 - methylene bis-(4,6-di-tert-butylphenyl) phosphate (also known as NA11) have been shown to increase the rate of crystallization as higher concentrations of nucleating agents are introduced.⁵⁹ Hence, it is thought that the catalyst residues particles here are not acting as nucleating agents.

Here it appears that only when samples are sheared, stretched polymer chains can adsorb onto these particles, which then act as heterogenous nucleation sites that lower the surface free energy of the critical nucleus. ^{15,17,18} At higher temperatures, heterogenous nucleation occurs more readily than homogenous nucleation, where for polypropylene it has been reported that heterogenous nucleation occurs in the temperature range of 60-150 °C. ^{15,16} In addition to undergoing heterogeneous primary nucleation, where the nucleation barrier is lowered in the presence of impurities, adsorption of stretched chains to catalyst residue particles has also been hypothesized to account for the large activation energy required to anneal away FIC precursors, even at temperatures above the equilibrium melting point. ²³

Shear-Induced Non-Isothermal Crystallization. In the previous section, we investigated the effect of specific work on the isothermal crystallization kinetics of polypropylene. Now, we look to explore the linear viscoelastic crystallization temperature as a function of specific work by monitoring the temperature at which the modulus crossover $(tan\delta = 1)$ occurs in a -1 °C/min temperature ramp.

Figure 4 shows the linear viscoelastic crystallization temperature versus specific work at two different shear rates for iPP6 and iPP7. As in the case of the isothermal crystallization kinetics, the FIC effects of iPP6 are considerably stronger than that of iPP7. At a shear rate of 0.3 s⁻¹, the

difference in the crystallization temperatures between iPP6 and iPP7 are more prominent compared to those at 1 s⁻¹ (see inset of Figure 4). Upon reaching higher levels of applied specific work, the linear viscoelastic crystallization temperatures of both samples appear to plateau with iPP6 always crystallizing at a higher temperature than iPP7 ($\Delta T > 0$). Here, it appears that higher particle concentrations do not affect the saturation level of specific work. It is thought that the nucleation ability of these particles diminishes with increasing shear rates (and specific work) as flow effects become more influential (see inset of Figure 4).

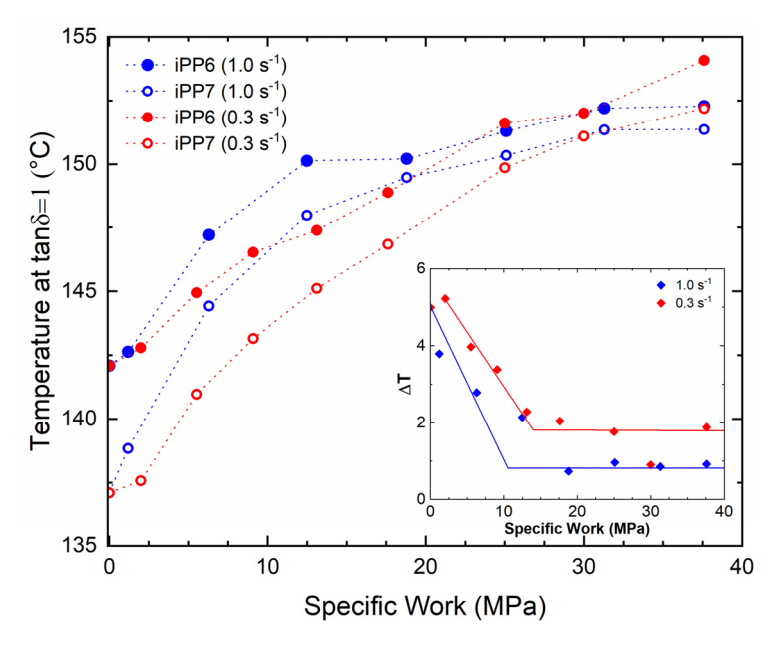


Figure 4. Crystallization temperature versus specific work at two shear rates (see legend) and shearing times for iPP6 and iPP7 using a shearing temperature of 170 °C and a cooling rate of 1 °C/min. The inset plot shows the temperature difference between iPP6 and iPP7 at the two shear rates.

Similar observations have also been made by D'Haese et al.^{60,61} during their birefringence experiments of polypropylene filled with different diameters of zinc oxide particles. The crystallization kinetics of the neat material and particle filled samples at low shear rates were more distinct, where the nucleating capability of the particles dominated. These differences weakened

with increasing shear rates, while within the high shear rate region, the crystallization kinetics were solely driven by flow and independent of the diameter and nucleating efficiently of their particles.

The increase in crystallization temperatures for shear rates of 0.3 and 1 s⁻¹ in Figure 4 is consistent with the hypothesis that stretched chains contribute strongly to FIC. As the shear rate increases, a greater fraction of the high molecular weight tails can be stretched by the flow (see Figure 1b). Thus, good overall agreement is seen for our samples sheared at higher rates, where FIC effects are generally stronger at 1 s⁻¹ than at 0.3 s⁻¹ for comparable specific work levels. Surprisingly, for the highest level of applied specific work (W = 38 MPa), the crystallization temperatures of iPP6 and iPP7 continue to increase when sheared at 0.3 s⁻¹, presumably due to the formation of shish-kebab structures, even in weak flow. To achieve this level of specific work at these low rates, the melt is sheared for long intervals of time. Here, only a small fraction of very long chains ($w_N = 4 \times 10^{-4}$; see Figure 1b) in the distribution are stretched, allowing for these chains to nucleate oriented shish precursors prior to crystallization.

Formation of Shish-kebab Structures at Low Shear Stress. The increase in dynamic modulus during crystallization is attributed to the rise of interconnected networks, or gelation, where the crystallites act as crosslinks connected by tie chains. In Figure 5a,b samples of iPP6 are normalized following the method developed by Winter and Pogodina, such that $G'_{norm} = \log(G'(T)/G'_{min})/\log(G'_{max}/G'_{min})$, where G'(T) is the storage modulus at intermediate temperatures, G'_{min} is storage modulus prior to crystallization, which is taken as the average storage modulus value of unsheared samples in the temperature range of 140 – 150 °C (0.025 MPa), while G'_{max} is approximated to be one-third (500 MPa) the reported Young's Modulus of polypropylene (~1.5 GPa)⁶² (see raw data and normalization in Figures S5 and S6). In all cases, the storage moduli evolve as crystals grow in the melt. Generally, upon the application of flow,

the curves of G' shift to higher temperatures and are accompanied by a change in slope for larger levels of specific work. For low levels of specific work (W < 7 MPa), the curves are shifted only to a minor degree, indicating a similar morphology as the case of quiescent crystallization. For specific work levels exceeding 13 MPa, the curves of G' exhibit a secondary slope change in moduli at low temperatures (see Figure 5b). This change in slope is perhaps due to an acceleration of nucleation from an increased number density of nuclei with increasing levels of specific work. Here, the morphology is transformed from spherulites to anisotropic shish-kebab structures, where the shift and slope change can be ascribed to crystalline lamella growing two dimensionally off a fibrillar structure.³ Indeed, the morphology of these shish-kebab structures will be elaborated on in the following sections through X-ray scattering.

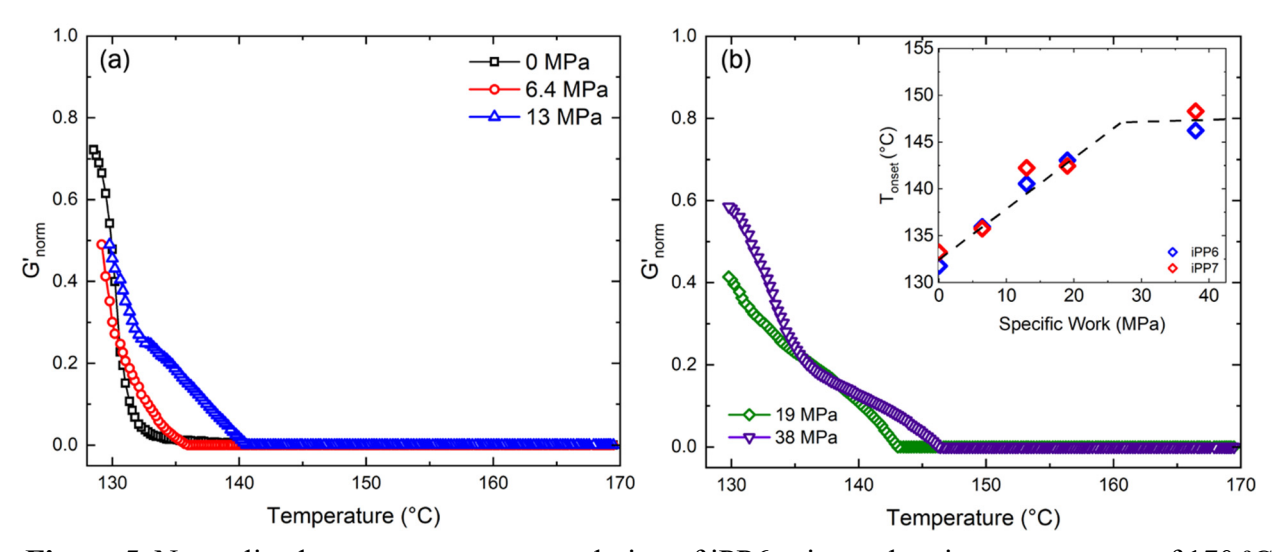


Figure 5. Normalized temperature ramp evolution of iPP6 using a shearing temperature of 170 °C at a shear rate of 0.2 s⁻¹ for various levels of applied specific work. The storage modulus at 1 rad/sec is monitored during cooling at 1 °C/min. (a) Specific work levels of 0, 6.4, and 13 MPa (b) Specific work levels of 19 and 38 MPa, where with increasing levels of deformation, a secondary change in slope indicates a transformation in morphology. The inset shows the onset temperature of both iPP6 and iPP7, both exhibiting similar crystallization onset temperatures at all specific work levels.

X-ray Scattering. *Ex-situ* simultaneous small- and wide-angle X-ray scattering (SAXS/WAXS) was employed to evaluate the effect of particle concentration on the evolution of

flow-induced lamellar structures with increasing levels of shear stress. Two sample sets of iPP6 and iPP7 were fabricated in *weak* and *strong* shear flow environments using 25 mm parallel plates. Weak shear flow samples were sheared at $T_s = 170$ °C for 4128 seconds at a low perimeter shear rate of 0.3 s⁻¹ prior to quenching to $T_c = 141$ °C (without undershooting) for crystallization using a cooling rate ~10 °C/min. The strong shear flow samples were sheared at a much higher perimeter shear rate of 145 s⁻¹ for 1 second and subsequently quenched to crystallization by bringing the samples to room temperature, using a cooling rate ~10 °C/min. Crystallization at $T_c = 141$ °C was bypassed in the case of strong shear flow, as structures formed under these large stress levels have been shown crystallize significantly at substantially higher temperatures.²⁵ Sheared polypropylene disks were prepared using 25 mm parallel plates, where the shear rate is linear in radial position from the center of the sample

$$\dot{\gamma} = \frac{\Omega r}{d} \tag{3}$$

$$\sigma = \dot{\gamma}\eta = \frac{\eta_0 \dot{\gamma}}{1 + (\dot{\gamma}\tau)^m} \tag{4}$$

where Ω is the angular rotation rate (rad/s), r is the radial position from the center of the sample, and d is the gap height between parallel plates. From equation 4, the shear stress at a given radial position can be calculated using the Cross model (Eq. 2; with m = 0.7).

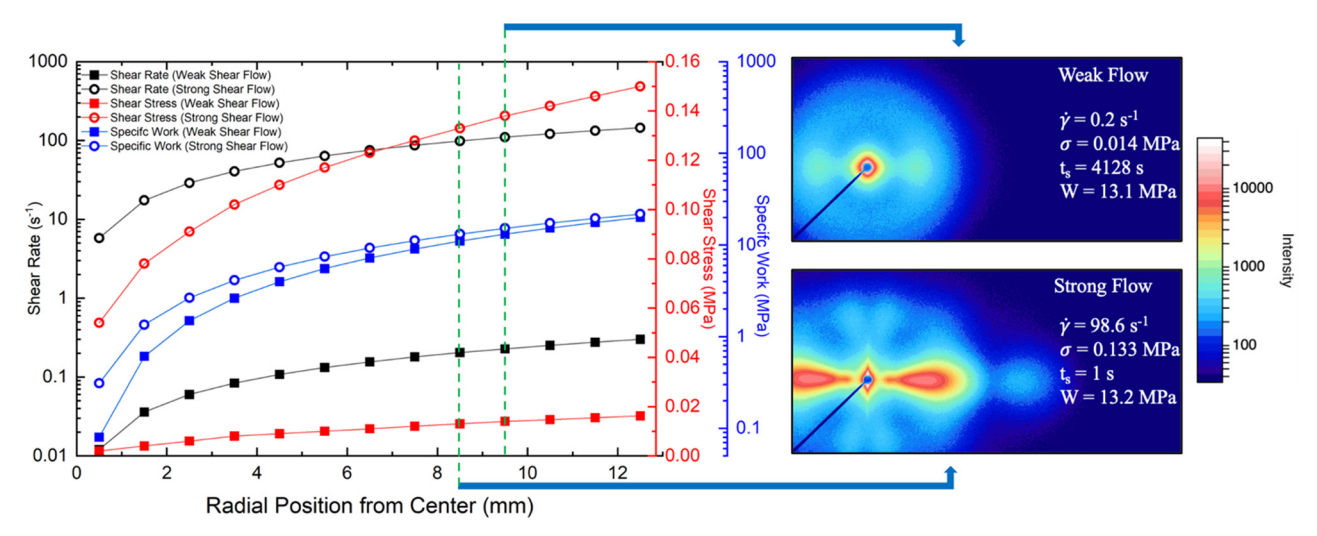


Figure 6. Process parameters (shear rate, shear stress, and specific work) as functions of radial position on the circular sample puck. The 2D SAXS images of iPP6 are shown in conditions of weak and strong shear flow at equivalent levels of specific work. While the strong flow samples (perimeter $\dot{\gamma} = 145 \text{ s}^{-1}$ for $t_s = 1 \text{ s}$) have a more anisotropic morphology, the weak flow sample (perimeter $\dot{\gamma} = 0.3 \text{ s}^{-1}$ for $t_s = 4128 \text{ s}$) also shows evidence of shish-kebab formation. In the intensity color bar, white is the highest intensity, followed by red, yellow, green, and blue. The flow direction is horizontal.

Figure 6 illustrates the different process parameters (shear rate, shear stress, and specific work) as functions of radial position on the parallel plate for the conditions of strong and weak flow. In this work, we will define three distinct morphology regimes consisting of: (1) quiescent crystallization; where $\dot{\gamma} < 1/\tau$, (2) the isotropic flow-induced regime ($\dot{\gamma} > 1/\tau$, for structures that have no visible orientation), and (3) the shish-kebab regime for structures with a high degree of anisotropic orientation (lobing) in stronger flows. We find that these shish-kebab structures can be induced in both strong and weak flow and will be a topic of discussion in the following sections.

The variable of specific work has often been thought to be a "universal parameter" for shish-kebab formation, 1,4,40 while at different degrees of deformation (for the same specific work levels) we show that these shish-kebab structures are qualitatively different in morphology (see right side of Figure 6).

Small-Angle X-ray Scattering Analysis. Shish-kebab Formation in Strong Shear Flow. Figure 7 qualitatively shows how shear affects the structural evolution of lamellar stacks at different radial positions on the sample disk. For relatively low levels of shear stress (Figure 7a, and 7f), the SAXS patterns are isotropic and show a random distribution of lamellae. Upon reaching a shear stress $\sigma = 0.102$ MPa, iPP6 shows the appearance of a meridional maximum (kebabs), while the corresponding structure for iPP7 is absent at the same stress level. The kebab structures of iPP6 form at a lower critical stress level and have a higher concentration of crystalline lamellae compared to iPP7. This is attributed to iPP6 having an increased concentration of particles, which increases the nucleation density of shish precursors, ultimately allowing for more accelerated growth of the kebab structures.

The formation of these shish-kebab structures is a two-step process. ²⁶ Deformation first forms a core fibrillar structure (shish) where these chain extended crystals then allow for folded-chain crystalline lamellae (kebabs) to grow epitaxially outward from the shish. Hsiao et al. used *in-situ* X-ray scattering to investigate the formation of shish-kebab structures in polypropylene and polyethylene. ^{26,28,29} In these studies, samples were sheared at 60 s⁻¹ for 5 seconds, where the initial scattering intensities were present in the flow direction, indicating the formation of shish structures. A few seconds thereafter, the crystalline lamellae (kebabs) could be seen growing perpendicular to the shish.

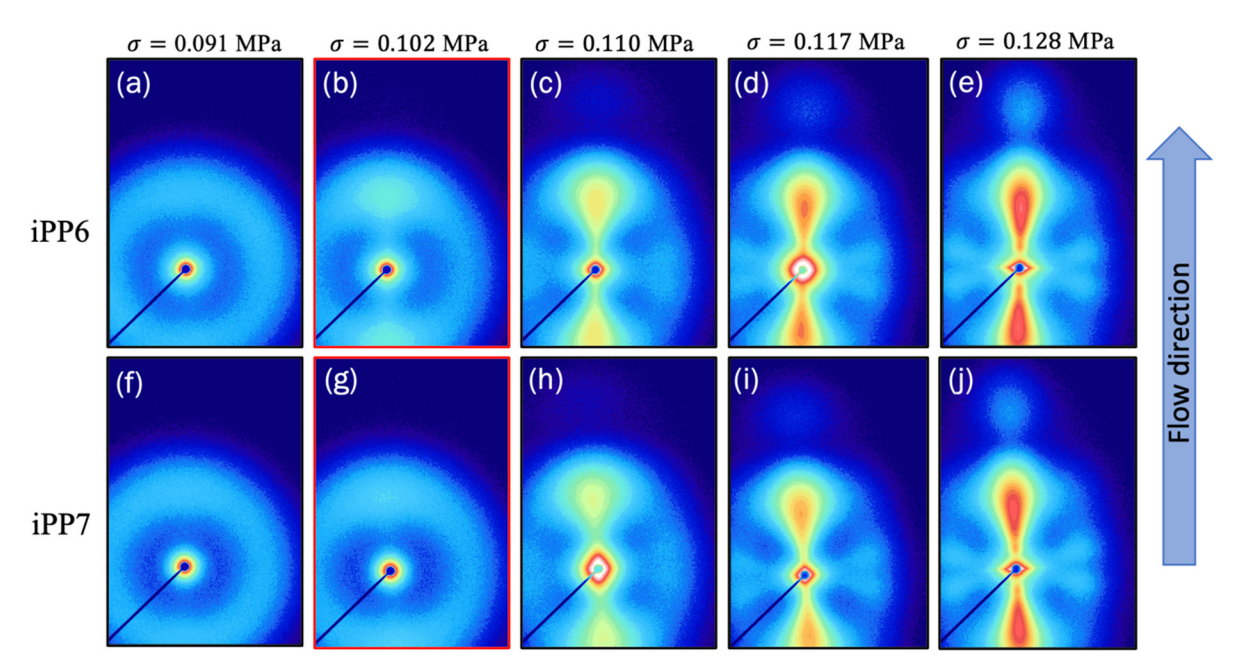


Figure 7. The onset and evolution of shish-kebab structures of iPP6 (top) and iPP7 (bottom) at five stress levels for strong shear flow with perimeter $\dot{\gamma} = 145 \text{ s}^{-1}$ for $t_s = 1 \text{ s}$. See Figure 6 for associated intensity colors.

Figure 8 illustrates a qualitative comparison of identically prepared sample pucks of iPP6 and iPP7 that were scanned in 1 mm increments to map the structural morphology as a function of increasing shear stress (and shear rate). The central regions of both sample disks show the presence of isotropic flow-induced structures (inside the solid green circles). From Figure 8b it is seen that iPP7 has a flow-induced crystallization (FIC) diameter of 8 mm, while iPP6 has a smaller FIC diameter of 6 mm, resulting in a lower critical shear rate (and shear stress) for the onset of shish-kebab formation. The critical shear rate ($\dot{\gamma}^*$) of iPP6 is ~35 s⁻¹, while that of iPP7 is ~46 s⁻¹. The corresponding critical shear stress (σ^*) necessary to induce shish-kebab structures for iPP6 and iPP7 are ~0.096 and ~0.106 MPa, respectively.

In knowing the respective flow-induced diameters, we can then calculate the relative amount of shish-kebab content present per sample disk in strong shear flow. The shish-kebab area per circular sample disk can be expressed as a percentage area of an annulus such that: $(R_{Outer}^2 - r_{Inner}^2)/(R_{Outer}^2)$, where R_{Outer} is the radius of the sample puck (12.5 mm) and r_{Inner} is the

respective interior flow-induced radius. Using this approach, we find that the sample disk of iPP6 is comprised of $\sim 94\%$ shish-kebab structures compared to $\sim 90\%$ for iPP7. It is evident that even small traces of catalyst residue play an integral role in promoting the formation of shish-kebab morphology. Mi et al. have reported that even small increases in shish-kebab content can improve mechanical properties. They found that with increasing shear layer thickness, the tensile and impact strengths increased, while the elongation at break decreased. 10

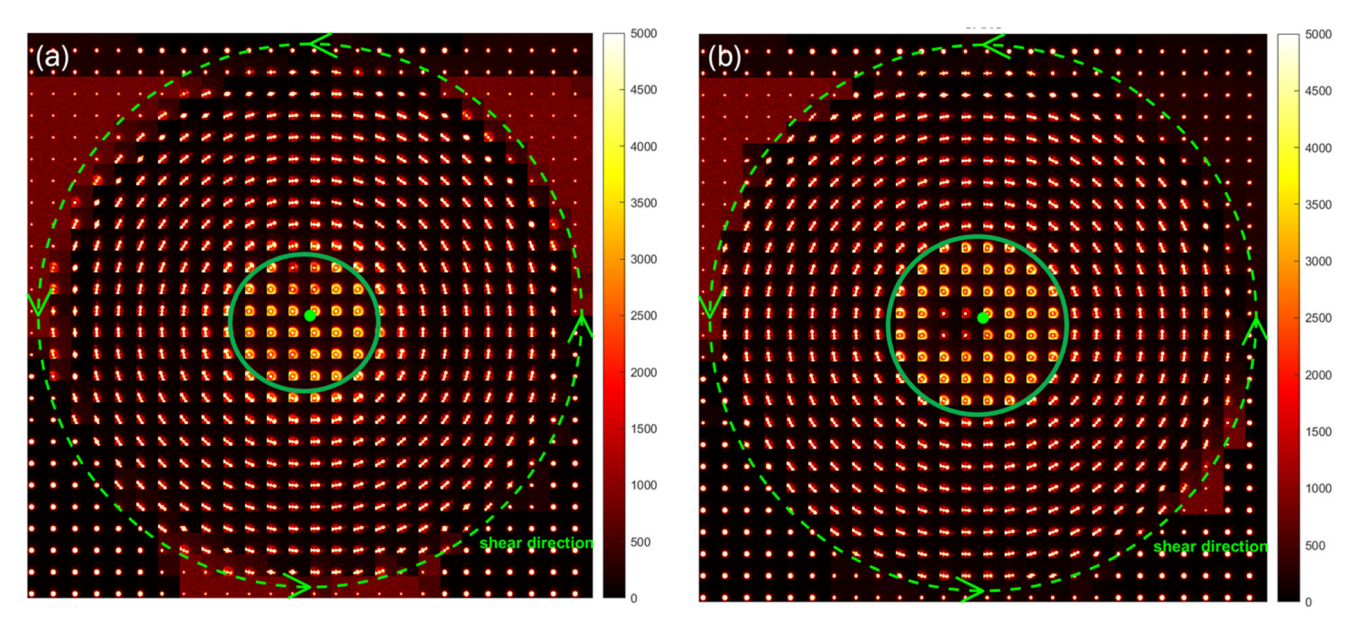


Figure 8. SAXS morphology evolution at different radial positions on a 25 mm diameter sample disk. Samples were subject to a perimeter shear rate of 145 s⁻¹ for 1 second at a temperature of 170°C. (a) iPP6 has a FIC diameter of 6 mm (solid green circle) resulting in a critical shear rate of ~35 s⁻¹ ($\sigma^* \sim 0.096$ MPa) for shish kebab formation (b) iPP7 has FIC diameter of 8 mm (solid green circle) resulting in a critical shear rate of ~46 s⁻¹ ($\sigma^* \sim 0.106$ MPa) for shish kebab formation.

From the evolutions of the shish-kebab structures in Figure 7, the initial ex-situ SAXS patterns show weak equatorial scattering corresponding to chain extended crystals. However, for shish-kebab structures formed at the highest shear stress $\sigma = 0.138$ MPa, a clear equatorial streak (shish) and very strong meridional scattering (kebabs) are observed in Figure 9. This suggests at low shear stresses that only a small fraction of chains contribute to the formation of shish, while with

increasing shear stresses a greater quantity of chains can be incorporated. For instance, at the edge of the parallel plate ($\dot{\gamma}$ = 145 s⁻¹), this stress level would correspond to a substantially higher weight fraction of stretched chains (w_N = 0.18), relative to lower shear rates (see Figure 1b).

With the formation of dense kebab structures ($\sigma > 0.11$ MPa), the 2D SAXS images show the development of higher order peaks. As the shear stress increases, the scattering intensity of these peaks becomes more prominent. In both samples, the intensity of these higher order peaks become similar to one another (see top of Figure 9), indicating that the spacing between the kebab structures are equivalent to one another.³²

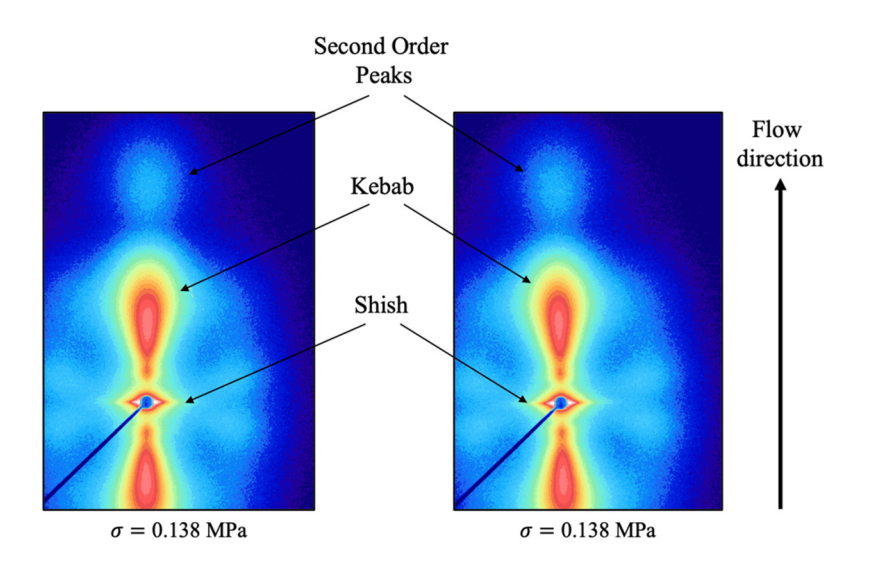


Figure 9. 2D SAXS images of sheared iPP6 (left) and iPP7 (right) at the highest stress level of $\sigma = 0.138$ MPa. In such strong flows, the flow effects dominate over the difference in particle concentrations. See Figure 6 for associated intensity colors.

Shish-kebab Formation in Weak Shear Flow. As illustrated in the previous section, the formation of shish-kebab structures are typically linked to intense deformations and high shear stresses. Figure 10 shows that these anisotropic structures can also arise in the presence of weak shear flow ($\dot{\gamma}_{perimeter} = 0.3 \text{ s}^{-1}$). When the shear stress reaches a value of $\sigma = 0.013 \text{ MPa}$, a qualitative change in morphology is seen in both samples, where the SAXS patterns show the

emergence of dense anisotropic lamellar crystals (kebab structures). As in the case of strong shear flow, the intensity of the kebab structures of iPP6 is greater than that of iPP7. In these samples, the *ex-situ* SAXS patterns also show weak equatorial scattering corresponding to shish, presumably due to the small fraction of chains that make up the shish.^{29,38,64} Nonetheless, the presence of shish can be indirectly inferred by the kebab structures, as the shish serve as nucleation sites for kebab growth.^{4,26,27,29,65,66}

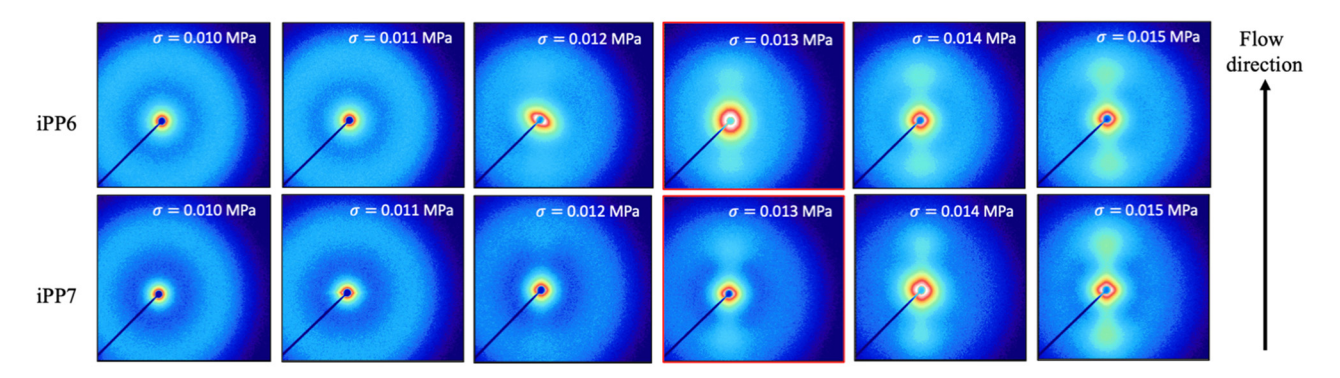


Figure 10. 2D SAXS pattern evolution of shish-kebab structures under weak shear flow (perimeter $\dot{\gamma} = 0.3 \text{ s}^{-1}$ with $t_s = 4128 \text{ s}$). As the threshold shear stress of 0.013 MPa, both samples show the onset of kebab formation. See Figure 6 for associated intensity colors.

In Figure 11 we present the shish-kebab morphology with a clear equatorial streak formed at a stress of $\sigma = 0.016$ MPa, indicating the robust presence of shish in both iPP6 and iPP7. Note that this stress level is induced closest to the edge of the parallel plate geometry, where flow-instabilities, such as edge fracture, are most pronounced. As such, quantitative analysis at this stress level ($\sigma = 0.016$ MPa) will be excluded in the following section due to the complexities of interpreting the scattering patterns affected by these flow-instabilities.

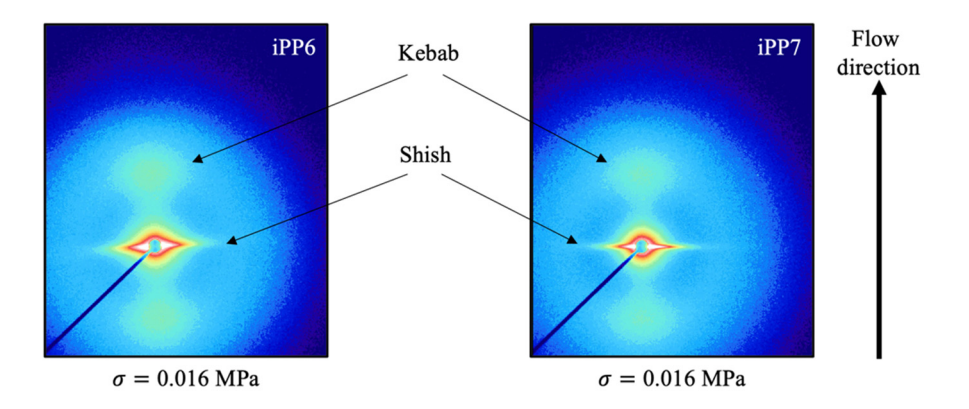


Figure 11. 2D SAXS images of sheared iPP6 and iPP7 at a corresponding stress level of $\sigma = 0.016$ MPa. The strong equatorial streak indicates shish formation, even at low shear stress, when sheared for long intervals of time (4128 sec). See Figure 6 for associated intensity colors.

A key feature of the present work is that both iPP6 and iPP7 are sheared above their nominal melting temperature ($T_m \sim 165$ °C), remarkably still allowing for the formation of stable shish precursors. Operating at these elevated shearing conditions ($T_s = 170$ °C) permits a clear separation of nuclei formation during flow, and the subsequent crystal growth upon cooling. It has been hypothesized that the stretched polymer chains adsorb onto the particle impurities within iPP6 and iPP7,²³ imparting unexpected stability to the FIC precursors.

In nearly all previous works, iPP has been sheared at relatively low temperatures (below the nominal melting point), where flow and crystallization effects can be indistinguishable. At these temperatures, nucleation is activated by both temperature and shear, allowing for rapid crystal growth during shear. Chains can be incorporated in multiple growing crystal nuclei that are then stretched by the flow as the nuclei separate, allowing for structures to be induced with high degrees of orientation. An an increase performed by Zhang et al., observed the formation of shish-kebab structures in weak flow ($\dot{\gamma} = 0.5 \text{ s}^{-1}$) of iPP when sheared at 140 °C. At temperatures below the melting point, it was suggested that a smectic ordered liquid

crystalline structure⁶⁸ or helical crystallite could be induced by shear flow through network stretching, subsequently allowing for adjacent chains to nucleate normal to the flow direction and form kebab structures.⁶⁷

In addition to particles stabilizing the melt in iPP6 and iPP7, it is thought that the long interval of shear ($t_s = 4128$ seconds) plays a vital role in forming these robust precursors. For polymer chains to be stretched by flow, the shear rate must be larger than that of the Rouse relaxation rate for the longest chains. Given that the shearing time is very long, stretched chains have sufficient time to find one another, or particles to adsorb to, and nucleate fibrillar shish structures that remain stable upon cessation of flow.^{37,38} The increased flow time allows for the formation of a stable nucleus even in the presence of weak flow, as enough chains can still be stretched and incorporated to form shish structures.^{4,38} Hence, for low levels of deformation, specific work has long been identified as an important parameter that governs the strength of flow-induced crystallization. Mykhaylyk et al. have even proposed that specific work is indeed the control variable for the formation of shish-kebabs.^{4,37} They interpreted that the stress component ($\sigma = \dot{\gamma}\eta$) is responsible for initially generating nucleating entities, while the strain ($\gamma = \dot{\gamma}t_s$), allows time for these objects to bundle together into a nucleus. However, Figure 6 clearly shows very different morphologies are formed at the same specific work level in weak and strong flows.

Lamellar Spacing. For quantitative analysis of the lamellar structure, the 2D SAXS images are reduced to 1D intensity profiles as a function of the scattering wavevector ($q = (4\pi/\lambda) \sin(\theta/2)$, where θ is the scattering angle and λ is the wavelength. Figure 12 shows the Lorentz-corrected^{69,70} (Iq²) intensity profiles as a function of shear stress for iPP6 (see Figure S7 for strong and weak shear flow comparison). Here, the data are circularly averaged over the

azimuthal angle to account for contributions that perhaps arise from parent and daughter lamellae.⁷⁰

As the shear stress increases, the scattering intensity becomes stronger and results in more ordered crystalline structures. Upon reaching a critical shear stress (~ 0.1 MPa), the positions of the structural peaks shift to smaller wavevector values as the kebab structures begin to grow. At this critical stress, second order scattering peaks appear at $q \sim 0.075$ A⁻¹, which are attributed to a high degree of chain alignment within the oriented crystals. Upon the formation of shish-kebab structures, we see two populations in the scattering profile of Figure 12, where the shoulder to the right of the kebab q_{max} peaks have similar spacings to structures formed at lower stress levels (~ 0.054 MPa). It could be thought that daughter crystals^{33,71} are formed epitaxially on the kebab structures, suggesting daughter crystals have similar spacings to isotropic crystals.

The long period, or spacing between crystalline lamellae, can be determined from the peak position of the intensity maxima (q_{max}) of the meridional SAXS patterns through $L_p=2\pi/q_{max}$. This represents the sum of the average crystal and amorphous layer thicknesses of the kebab structures that dominate the semicrystalline morphology.⁷²

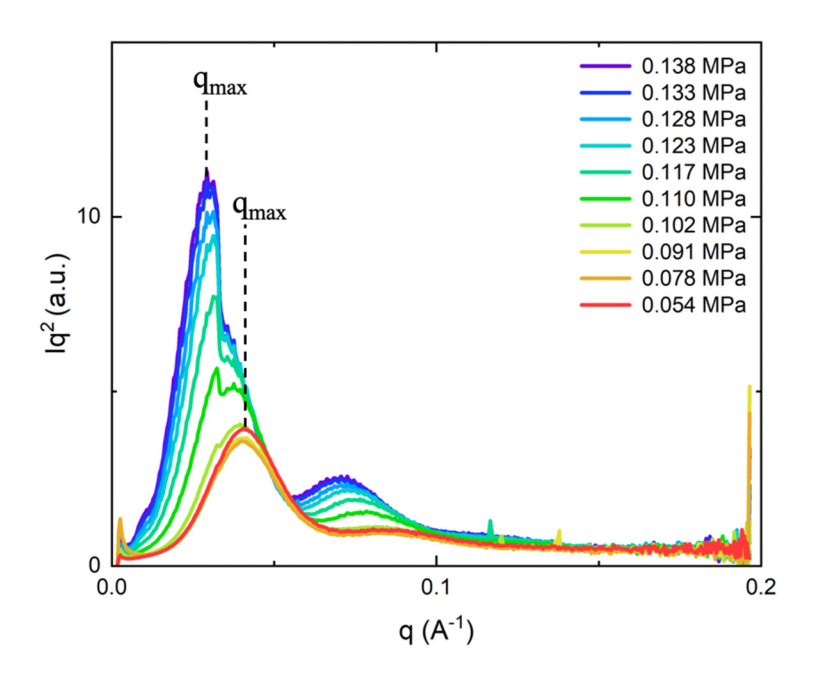


Figure 12. SAXS Lorentz-corrected intensity profiles of iPP6. This sample was subject to strong shear at $T_s = 170$ °C with a perimeter shear rate of 145 s⁻¹ ($t_s = 1$ second) and quenched to crystallization. With increasing shear stress, the scattering peaks become sharper and shift to lower wavevector values, increasing the long period.

crystallinity (blue markers) in weak and strong shear flow. For quiescent conditions (σ < 0.009 MPa), the long periods of iPP6 and iPP7 were found to be 170 Å and 163 Å, respectively. In weak shear flow (Figure 13a) these long periods are maintained until a stress of 0.01 MPa is exceeded. Thereafter, iPP6 has a noticeable upturn in lamellar spacing, reaching a value of L_p = 194 Å, indicating the formation of shish-kebab structures, even in the presence of weak shear flow. This is further corroborated by a *characteristic comparison* of the long period of shish-kebab structures formed in strong shear flow (σ > 0.05 MPa) as seen in Figure 13b. At the critical shear stress of ~0.1 MPa, an abrupt jump in the lamellar spacing is observed for both iPP6 and iPP7, with iPP6 once again exhibiting a distinctive long period value of L_p = 194 Å. Notably, we also find that the long period values of iPP6 and iPP7 at σ = 0.015 MPa exceed those of the highest shear stress (σ = 0.138 MPa) by nearly 15 Å.

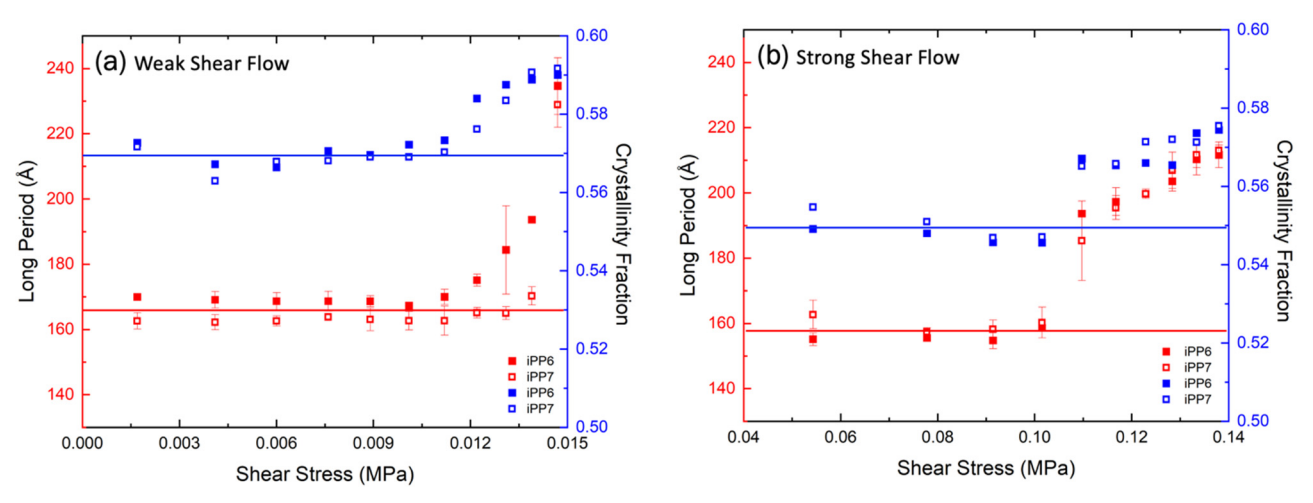


Figure 13. Shear stress evolution of lamellar spacing (red) and degree of crystallinity (blue) for iPP6 (solid markers) and iPP7 (open markers). (a) Structure development in weak shear flow. Samples were sheared at $T_s = 170$ °C with a perimeter $\dot{\gamma} = 0.3$ s⁻¹ and crystallized at $T_c = 141$ °C to ensure crystallization of weakly oriented structures. (b) Structure development in strong shear flow. Samples were sheared at $T_s = 170$ °C with a perimeter $\dot{\gamma} = 145$ s⁻¹ and subsequently quenched to crystallization. Using 25 mm parallel plates, the long period results were averaged between four of the same radial positions, with the error bars denoting the standard deviation. With weak shear flow, the long period starts to increase at an order of magnitude lower shear stress than in 1 s of strong shearing.

Given that both sample sets were prepared with different process parameters, the long period and degree of crystallinity in both sample sets exhibit distinct characteristics. In the weak flow regime, the long period of iPP6 consistently exceeds that of iPP7, while in strong flow, these values converge. From Figure 13a, the larger lamellar spacing observed in iPP6 is attributed to a higher nucleation density, perhaps arising from the increased concentration of catalyst residue particles. This is consistent with the impact that nucleating agents have on the flow-induced crystallization of isotactic polypropylene. Balzano et al.⁷³ found that samples of isotactic polypropylene with higher concentrations of nucleating agents resulted in larger lamellar spacings, which was also accredited to the formation of thicker crystals in the presence of these nucleating agents.

At sufficiently high shear stress levels (Figure 13b), flow effects are predominant. The increase in length scales of the lamellar structure can be ascribed to a higher fraction of chains that are stretched and oriented by the flow. As the shear rate increases, a greater proportion of long chains can be incorporated into the crystal fraction, resulting in longer relaxation times and sustained orientation. Shorter chains, however, relax at a much faster rate upon cessation of shear, leading to more uniform length scales.³⁸

Wide-Angle X-ray Scattering Analysis. Upon converting the 2D WAXS patterns to 1D Intensity profiles, the degree of crystallinity (χ_c) was obtained by fitting the crystalline peaks and amorphous halo to Gaussian functions upon performing a baseline correction (see Figure S8), such that:

$$\chi_{\rm c} = \frac{I_{crystal}}{I_{crystal} + I_{amorphous}} \tag{5}$$

where $I_{crystal}$ is the total integrated intensity of α , β , and γ crystalline peaks, and $I_{amorphous}$ the integrated intensity of the amorphous halo. The five predominant α phase reflections are: (110) at $q = 1.0 \text{ Å}^{-1}$, (040) at $q = 1.19 \text{ Å}^{-1}$, (130) at $q = 1.31 \text{ Å}^{-1}$, (111) at $q = 1.49 \text{ Å}^{-1}$, and (131) at $q = 1.53 \text{ Å}^{-1}$. It should also be noted that many of these α crystalline peaks can have contributions of β and γ crystalline fractions, while the (130) reflection consists exclusively of α phase crystals. The reflections assigned exclusively to β and γ crystalline fractions are (300) at $q = 1.13 \text{ Å}^{-1}$ and (117) at $q = 1.41 \text{ Å}^{-1}$, respectively (see Figure S9 for comparison of WAXS profiles).

The evolution of the degree of crystallinity for iPP6 and iPP7 as a function of shear stress is also shown in Figure 13 (blue markers). In weak shear flow, the overall crystallinity fractions are higher than that of strong shear flow, which is due to the longer duration of time required to completely crystallize the structures formed under low shear stress. Here, polymer chains have increased mobility and more time to organize and pack into crystals, leading to overall larger levels of crystallinity. Nonetheless, we find that upon formation of shish-kebab structures in both flow regimes, the degree of crystallinity progressively increases with applied shear stress. In weak flow this change is gradual, while with strong shear flow an abrupt jump in crystallinity is seen when the shear stress exceeds ~0.1 MPa. Transitioning from the flow-induced regime to the shish-kebab regime, the degree of crystallinity raises by ~2%. This is perhaps driven by the perfect lattice matching ability between shish crystals and lamellar kebab structures, which has been suggested to promote crystallinity. In both cases of weak and strong shear flow, the crystallinity of iPP6 and iPP7 are approximately the same for all stress levels, due to both samples having similar tacticities.

CONCLUSIONS

The flow-induced crystallization of two high molecular weight samples of isotactic polypropylene with differing concentrations of catalyst residue was investigated. Both samples are polydisperse with $M_w = 656$ kg/mol, obtained from the zero shear rate viscosity for entangled linear polymer melts.⁴² The samples have identical viscoelastic responses, and nearly indistinguishable high molecular weight tails that contain only linear chains. Using a rotational rheometer, we investigated how the isothermal flow-induced crystallization kinetics and crystallization temperatures upon cooling evolve with increasing levels of applied specific work. Synchrotron X-ray scattering was used to map the structural morphology and transition in crystalline microstructure of sheared samples.

For both samples, we find that the crystallization rate increases with applied specific work until a saturation threshold is reached, where FIC remains relatively constant as specific work is further increased, possibly set by reaching a maximum number density of nuclei for the given levels of deformation. Similarly, we find that the linear viscoelastic crystallization temperature shifts to higher temperatures with increasing levels of deformation. In both cases, the sample with higher particle concentrations resulted in faster crystallization kinetics and crystallized at higher temperatures for all levels of applied specific work. The crystallization times from quiescent crystallization to the maximum specific work applied decreased by a factor of ~335 for iPP6, while in the same range iPP7 decreased by a factor of ~170. The effect of increased particle concentration on FIC was more profound for lower levels of deformation, while flow effects became predominant with larger deformations. Upon the formation of shish-kebab structures, it is thought

that the effect of particles becomes inconsequential, while the shish structures serve as a better nucleation mechanism relative to polymer chains adsorbing onto these heterogenous impurities.

The flow-induced morphology was investigated in conditions of weak and strong shear flow. In strong shear flow (perimeter $\dot{\gamma}=145~{\rm s}^{-1}$ for $t_s=1~{\rm s}$), we find that the sample with higher concentrations of particles formed shish-kebab structures at a lower critical shear stress (~0.096 MPa) and resulted in an approximately 4% increase in shish-kebab content per sample disk compared to the sample with fewer particles. Although typically linked to large deformations, remarkably, we have also uncovered the formation of these anisotropic structures in the presence of weak shear flow (perimeter $\dot{\gamma}=0.3~{\rm s}^{-1}$ for $t_s=4128~{\rm s}$) when sheared for long intervals of time. For equivalent levels of specific work within these two flow regimes, the structural morphologies of the shish-kebab structures were found to be characteristically distinct from one another. The spacing between adjacent lamella and degree of crystallinity were also found to increase with shear stress upon the formation of shish-kebab structures. This is due to the near perfect chain-extended conformation of the shish interface, which can serve as a substrate to promote crystallization and thicker interlamellar layers, driven by specific work, either from large deformation rates very long or durations of shear at lower shear rates.

ASSOCIATED CONTENT

Supporting Information

Details of GPC, rheology, and thermal analysis experiments. The raw data for temperature ramps and extraction of the crystallization onset temperature; SAXS and WAXS data analysis are also presented.

AUTHOR INFORMATION

Corresponding Authors

Alicyn M. Rhoades – School of Engineering, Penn State Behrend, Erie, Pennsylvania 16563, United States; orcid.org/0000-0003-4678-419X; Email: amh234@psu.edu

Ralph H. Colby – Department of Materials Science and Engineering, The Pennsylvania State University, University Park, Pennsylvania 16802, United States; orcid.org/0000-0002-5492-6189;

Email: <u>rhc@plmsc.psu.edu</u>

Authors

Benson J. Jacob – Department of Chemical Engineering, The Pennsylvania State University, University Park, Pennsylvania 16802, United States

Xiaoshi Zhang – School of Engineering, Penn State Behrend, Erie, Pennsylvania 16563, United States

Jongkyeong Kim – Department of Materials Science and Engineering, The Pennsylvania State University, University Park, Pennsylvania 16802, United States

Jason D. Alexander – Department of Chemical Engineering, The Pennsylvania State University, University Park, Pennsylvania 16802, United States

Manoela E. Cangussú – Braskem Innovation and Technology Center, Via Oeste, Lote 5, Passo Raso, Triunfo, 95853, RS, Brazil

ACKNOWLEDGMENTS

The authors acknowledge support from the National Science Foundation (DMR-2218775). We thank Jerry Magraw (Penn State Behrend) for performing ICP-MS on the samples used in this study. We would also like to thank the DuPont-Northwestern-Dow Collaborative Access Team (DND-CAT) located at Sector 5 of the Advanced Photon Source (APS) at Argonne National Laboratory (ANL). The authors also thank Dr. Darren Pagan (Penn State Material Science and Engineering) for helpful discussions on the X-ray scattering analysis, and Douglas Harrell from Phillips 66 for providing the samples of polypropylene used in this work.

REFERENCES

- (1) Janeschitz-Kriegl, H.; Ratajski, E. Some Fundamental Aspects of the Kinetics of Flow-Induced Crystallization of Polymers. *Colloid Polym. Sci.* **2010**, *288* (16–17), 1525–1537.
- (2) Janeschitz-Kriegl, H. Some Remarks on Flow Induced Crystallization in Polymer Melts. *J. Rheol.* **2013**, *57* (4), 1057–1064.
- (3) Housmans, J.-W.; Steenbakkers, R. J. A.; Roozemond, P. C.; Peters, G. W. M.; Meijer, H. E. H. Saturation of Pointlike Nuclei and the Transition to Oriented Structures in Flow-Induced Crystallization of Isotactic Polypropylene. *Macromolecules* **2009**, *42* (15), 5728–5740.
- (4) Mykhaylyk, O. O.; Chambon, P.; Impradice, C.; Fairclough, J. P. A.; Terrill, N. J.; Ryan, A. J. Control of Structural Morphology in Shear-Induced Crystallization of Polymers. *Macromolecules* **2010**, *43* (5), 2389–2405.
- (5) Kumaraswamy, G.; Issaian, A. M.; Kornfield, J. A. Shear-Enhanced Crystallization in Isotactic Polypropylene. 1. Correspondence between in Situ Rheo-Optics and Ex Situ Structure Determination. *Macromolecules* **1999**, *32* (22), 7537–7547.
- (6) Janeschitz-Kriegl, H. An Unusual but Consistent View on Flow Induced Crystallization of Polymers. *Monatshefte Für Chem. Chem. Mon.* **2007**, *138* (4), 327–335.
- (7) Pogodina, N. V.; Winter, H. H.; Srinivas, S. Strain Effects on Physical Gelation of Crystallizing Isotactic Polypropylene. *J. Polym. Sci. Part B Polym. Phys.* **1999**, *37* (24), 3512–3519.
- (8) Cui, K.; Ma, Z.; Tian, N.; Su, F.; Liu, D.; Li, L. Multiscale and Multistep Ordering of Flow-Induced Nucleation of Polymers. *Chem. Rev.* **2018**, *118* (4), 1840–1886.
- (9) Nie, C.; Peng, F.; Cao, R.; Cui, K.; Sheng, J.; Chen, W.; Li, L. Recent Progress in Flow-Induced Polymer Crystallization. *J. Polym. Sci.* **2022**, *60* (23), 3149–3175.
- (10) Mi, D.; Xia, C.; Jin, M.; Wang, F.; Shen, K.; Zhang, J. Quantification of the Effect of Shish-Kebab Structure on the Mechanical Properties of Polypropylene Samples by Controlling Shear Layer Thickness. *Macromolecules* 2016, 49 (12), 4571–4578.
- (11) Zhou, D.; Yang, S.-G.; Lei, J.; Hsiao, B. S.; Li, Z.-M. Role of Stably Entangled Chain Network Density in Shish-Kebab Formation in Polyethylene under an Intense Flow Field. *Macromolecules* **2015**, *48* (18), 6652–6661.
- (12) Coppola, S.; Grizzuti, N.; Maffettone, P. L. Microrheological Modeling of Flow-Induced Crystallization. *Macromolecules* **2001**, *34* (14), 5030–5036.
- (13) Seo, J.; Gohn, A. M.; Schaake, R. P.; Parisi, D.; Rhoades, A. M.; Colby, R. H. Shear Flow-Induced Crystallization of Poly(Ether Ether Ketone). *Macromolecules* **2020**, *53* (9), 3472–3481.
- (14) Hoffman, J. D.; Lauritzen, J. I. Crystallization of Bulk Polymers With Chain Folding: Theory of Growth of Lamellar Spherulites. *J. Res. Natl. Bur. Stand. Sect. Phys. Chem.* **1961**, 65A (4), 297–336.
- (15) Howard, M. P.; Milner, S. T. A Simple Model for Heterogeneous Nucleation of Isotactic Polypropylene. *Macromolecules* **2013**, *46* (16), 6593–6599.
- (16) De Santis, F.; Adamovsky, S.; Titomanlio, G.; Schick, C. Isothermal Nanocalorimetry of Isotactic Polypropylene. *Macromolecules* **2007**, *40* (25), 9026–9031.

- (17) Howard, M. P.; Milner, S. T. Calculated Interfacial Free Energies and Hetrogeneous Nucleation of Isotactic Polypropylene. *Macromolecules* **2013**, *46* (16), 6600–6612.
- (18) Hamad, F. G.; Colby, R. H.; Milner, S. T. Onset of Flow-Induced Crystallization Kinetics of Highly Isotactic Polypropylene. *Macromolecules* **2015**, *48* (11), 3725–3738.
- (19) Wittmann, J. C.; Lotz, B. Epitaxial Crystallization of Polymers on Organic and Polymeric Substrates. *Prog. Polym. Sci.* **1990**, *15* (6), 909–948.
- (20) Wittmann, J. C.; Lotz, B. Epitaxial Crystallization of Polyethylene on Organic Substrates: A Reappraisal of the Mode of Action of Selected Nucleating Agents. *J. Polym. Sci. Polym. Phys. Ed.* **1981**, *19* (12), 1837–1851.
- (21) Kumaraswamy, G.; Verma, R. K.; Issaian, A. M.; Wang, P.; Kornfield, J. A.; Yeh, F.; Hsiao, B. S.; Olley, R. H. Shear-Enhanced Crystallization in Isotactic polypropylenePart 2. Analysis of the Formation of the Oriented "Skin." *Polymer* **2000**, *41* (25), 8931–8940.
- (22) Vleeshouwers, S.; Meijer, H. E. H. A Rheological Study of Shear Induced Crystallization. *Rheol. Acta* **1996**, *35* (5), 391–399.
- (23) Hamad, F. G.; Colby, R. H.; Milner, S. T. Lifetime of Flow-Induced Precursors in Isotactic Polypropylene. *Macromolecules* **2015**, *48* (19), 7286–7299.
- (24) Hamad, F. G.; Colby, R. H.; Milner, S. T. Transition in Crystal Morphology for Flow-Induced Crystallization of Isotactic Polypropylene. *Macromolecules* **2016**, *49* (15), 5561–5575.
- (25) Nazari, B.; Tran, H.; Beauregard, B.; Flynn-Hepford, M.; Harrell, D.; Milner, S. T.; Colby, R. H. Two Distinct Morphologies for Semicrystalline Isotactic Polypropylene Crystallized after Shear Flow. *Macromolecules* **2018**, *51* (13), 4750–4761.
- (26) Somani, R. H.; Yang, L.; Zhu, L.; Hsiao, B. S. Flow-Induced Shish-Kebab Precursor Structures in Entangled Polymer Melts. *Polymer* **2005**, *46* (20), 8587–8623.
- (27) Balzano, L.; Ma, Z.; Cavallo, D.; van Erp, T. B.; Fernandez-Ballester, L.; Peters, G. W. M. Molecular Aspects of the Formation of Shish-Kebab in Isotactic Polypropylene. *Macromolecules* 2016, 49 (10), 3799–3809.
- (28) Hsiao, B. S.; Yang, L.; Somani, R. H.; Avila-Orta, C. A.; Zhu, L. Unexpected Shish-Kebab Structure in a Sheared Polyethylene Melt. *Phys. Rev. Lett.* **2005**, *94* (11), 117802.
- (29) Somani, R. H.; Hsiao, B. S.; Nogales, A.; Srinivas, S.; Tsou, A. H.; Sics, I.; Balta-Calleja, F. J.; Ezquerra, T. A. Structure Development during Shear Flow-Induced Crystallization of i-PP: In-Situ Small-Angle X-Ray Scattering Study. *Macromolecules* **2000**, *33* (25), 9385–9394.
- (30) Nogales, A.; Hsiao, B. S.; Soman, R. H.; Srinivas, S.; Tsou, A. H.; Balta-Calleja, F. J.; Ezquerrab, T. A. Shear-Induced Crystallization of Isotactic Polypropylene with Different Molecular Weight Distributions: In Situ Small- and Wide-Angle X-Ray Scattering Studies. *Polymer* **2001**, *42*, 5247–5256.
- (31) Ma, Z.; Balzano, L.; Van Erp, T.; Portale, G.; Peters, G. W. M. Short-Term Flow Induced Crystallization in Isotactic Polypropylene: How Short Is Short? *Macromolecules* **2013**, *46* (23), 9249–9258.
- (32) Somani, R. H.; Yang, L.; Hsiao, B. S. Effects of High Molecular Weight Species on Shear-Induced Orientation and Crystallization of Isotactic Polypropylene. *Polymer* **2006**, *47* (15), 5657–5668.
- (33) Troisi, E. M.; Caelers, H. J. M.; Peters, G. W. M. Full Characterization of Multiphase, Multimorphological Kinetics in Flow-Induced Crystallization of IPP at Elevated Pressure. *Macromolecules* **2017**, *50* (10), 3868–3882.

- (34) Fernandez-Ballester, L.; Thurman, D. W.; Zhou, W.; Kornfield, J. A. Effect of Long Chains on the Threshold Stresses for Flow-Induced Crystallization in iPP: Shish Kebabs vs Sausages. *Macromolecules* **2012**, *45* (16), 6557–6570.
- (35) Progress in Understanding of Polymer Crystallization; Reiter, G., Strobl, G. R., Eds.; Lecture Notes in Physics; Springer Berlin Heidelberg: Berlin, Heidelberg, 2007; Vol. 714.
- (36) Acierno, S.; Palomba, B.; Winter, H. H.; Grizzuti, N. Effect of Molecular Weight on the Flow-Induced Crystallization of Isotactic Poly(1-Butene). *Rheol. Acta* **2003**, *42* (3), 243–250.
- (37) Mykhaylyk, O. O.; Chambon, P.; Graham, R. S.; Fairclough, J. P. A.; Olmsted, P. D.; Ryan, A. J. The Specific Work of Flow as a Criterion for Orientation in Polymer Crystallization. *Macromolecules* **2008**, *41* (6), 1901–1904.
- (38) Seo, J.; Parisi, D.; Gohn, A. M.; Han, A.; Song, L.; Liu, Y.; Schaake, R. P.; Rhoades, A. M.; Colby, R. H. Flow-Induced Crystallization of Poly(Ether Ether Ketone): Universal Aspects of Specific Work Revealed by Corroborative Rheology and X-Ray Scattering Studies. *Macromolecules* **2020**, *53* (22), 10040–10050.
- (39) Janeschitz-Kriegl, H.; Ratajski, E. Kinetics of Polymer Crystallization under Processing Conditions: Transformation of Dormant Nuclei by the Action of Flow. *Polymer* No. 46, 3856–3870.
- (40) Janeschitz-Kriegl, H. *Crystallization Modalities in Polymer Melt Processing*; Springer International Publishing: Cham, 2018.
- (41) Okura, M.; Chambon, P.; Mykhaylyk, O. O.; Fairclough, J. P. A.; Ryan, A. J. Using Multimodal Blends to Elucidate the Mechanism of Flow-Induced Crystallization in Polymers. *J. Polym. Sci. Part B Polym. Phys.* **2011**, *49* (9), 621–628.
- (42) Parisi, D.; Han, A.; Seo, J.; Colby, R. H. Rheological Response of Entangled Isotactic Polypropylene Melts in Strong Shear Flows: Edge Fracture, Flow Curves, and Normal Stresses. *J. Rheol.* **2021**, *65* (4), 605–616.
- (43) Yu, Y.; DesLauriers, P. J.; Rohlfing, D. C. SEC-MALS Method for the Determination of Long-Chain Branching and Long-Chain Branching Distribution in Polyethylene. *Polymer* **2005**, *46* (14), 5165–5182.
- (44) Gloger, D.; Mileva, D.; Albrecht, A.; Hubner, G.; Androsch, R.; Gahleitner, M. Long-Chain Branched Polypropylene: Effects of Chain Architecture, Melt Structure, Shear Modification, and Solution Treatment on Melt Relaxation Dynamics. *Macromolecules* **2022**, *55* (7), 2588–2608.
- (45) Dockhorn, R.; Plüschke, L.; Geisler, M.; Zessin, J.; Lindner, P.; Mundil, R.; Merna, J.; Sommer, J.-U.; Lederer, A. Polyolefins Formed by Chain Walking Catalysis—A Matter of Branching Density Only? J. Am. Chem. Soc. 2019, 141 (39), 15586–15596.
- (46) Orski, S. V.; Kassekert, L. A.; Farrell, W. S.; Kenlaw, G. A.; Hillmyer, M. A.; Beers, K. L. Design and Characterization of Model Linear Low-Density Polyethylenes (LLDPEs) by Multidetector Size Exclusion Chromatography. *Macromolecules* **2020**, *53* (7), 2344–2353.
- (47) Cangussú, M. E.; de Azeredo, A. P.; Simanke, A. G.; Monrabal, B. Characterizing Long Chain Branching in Polypropylene. *Macromol. Symp.* **2018**, *377* (1), 1700021.
- (48) Zimm, B. H.; Stockmayer, W. H. The Dimensions of Chain Molecules Containing Branches and Rings. *J. Chem. Phys.* **1949**, *17* (12), 1301–1314.
- (49) Pogodina, N. V.; Winter, H. H. Polypropylene Crystallization as a Physical Gelation Process. *Macromolecules* **1998**, *31* (23), 8164–8172.

- (50) Iijima, M.; Strobl, G. Isothermal Crystallization and Melting of Isotactic Polypropylene Analyzed by Time- and Temperature-Dependent Small-Angle X-Ray Scattering Experiments. *Macromolecules* **2000**, *33* (14), 5204–5214.
- (51) Natta, G.; Corradini, P. Structure and Properties of Isotactic Polypropylene. *Il Nuovo Cimento 1955-1965* **1960**, *15* (1), 40–51.
- (52) Striegel, A. M.; Wallace W. Yau; Joseph J. Kirkland; Donald D. Bly. *Modern Size-Exclusion Liquid Chromatography*, 2nd ed.; John Wiley & Sons, Ltd, 2009.
- (53) Kimata, S.; Sakurai, T.; Nozue, Y.; Kasahara, T.; Yamaguchi, N.; Karino, T.; Shibayama, M.; Kornfield, J. A. Molecular Basis of the Shish-Kebab Morphology in Polymer Crystallization. *Science* 2007, 316 (5827), 1014–1017.
- (54) Doi, M.; Edwards, S. F. *The Theory of Polymer Dynamics*; Oxford University Press: New York, 1986.
- (55) Rubinstein, M.; Colby, R. H. *Polymer Physics*; Oxford University Press: New York, 2003.
- (56) Fetters, L. J.; Lohse, D. J.; Graessley, W. W. Chain Dimensions and Entanglement Spacings in Dense Macromolecular Systems. *J. Polym. Sci. Part B Polym. Phys.* **1999**, *37* (10), 1023–1033.
- (57) Cross, M. M. Rheology of Non-Newtonian Fluids: A New Flow Equation for Pseudoplastic Systems. *J. Colloid Sci.* **1965**, *20* (5), 417–437.
- (58) Cox, W. P.; Merz, E. H. Correlation of Dynamic and Steady Flow Viscosities. *J. Polym. Sci.* **1958**, *28* (118), 619–622.
- (59) Patil, N.; Invigorito, C.; Gahleitner, M.; Rastogi, S. Influence of a Particulate Nucleating Agent on the Quiescent and Flow-Induced Crystallization of Isotactic Polypropylene. *Polymer* **2013**, *54* (21), 5883–5891.
- (60) D'Haese, M.; Van Puyvelde, P.; Langouche, F. Effect of Particles on the Flow-Induced Crystallization of Polypropylene at Processing Speeds. *Macromolecules* **2010**, *43* (6), 2933–2941.
- (61) D'Haese, M.; Langouche, F.; Van Puyvelde, P. On the Effect of Particle Size, Shape, Concentration, and Aggregation on the Flow-Induced Crystallization of Polymers. *Macromolecules* **2013**, *46* (9), 3425–3434.
- (62) Li, J.; Zhu, Z.; Li, T.; Peng, X.; Jiang, S.; Turng, L.-S. Quantification of the Young's Modulus for Polypropylene: Influence of Initial Crystallinity and Service Temperature. *J. Appl. Polym. Sci.* **2020**, *137* (16), 48581.
- (63) van Erp, T. B.; Balzano, L.; Peters, G. W. M. Oriented Gamma Phase in Isotactic Polypropylene Homopolymer. *ACS Macro Lett.* **2012**, *I* (5), 618–622.
- (64) Matsuba, G.; Ito, C.; Zhao, Y.; Inoue, R.; Nishida, K.; Kanaya, T. In Situ Small-Angle X-Ray and Neutron Scattering Measurements on a Blend of Deuterated and Hydrogenated Polyethylenes during Uniaxial Drawing. *Polym. J.* **2013**, *45* (3), 293–299.
- (65) Deng, B.; Chen, L.; Li, X.; Wang, Z. Influence of Prereserved Shish Crystals on the Structural Evolution of Ultrahigh-Molecular Weight Polyethylene Films during the Hot Stretching Process. *Macromolecules* **2022**, *55* (11), 4600–4613.
- (66) Dukovski, I.; Muthukumar, M. Langevin Dynamics Simulations of Early Stage Shish-Kebab Crystallization of Polymers in Extensional Flow. *J. Chem. Phys.* **2003**, *118* (14), 6648–6655.
- (67) Zhang, C.; Hu, H.; Wang, D.; Yan, S.; Han, C. C. In Situ Optical Microscope Study of the Shear-Induced Crystallization of Isotactic Polypropylene. *Polymer* **2005**, *46*, 8157–8161.

- (68) Li; de Jeu, W. H. Shear-Induced Smectic Ordering as a Precursor of Crystallization in Isotactic Polypropylene. *Macromolecules* **2003**, *36* (13), 4862–4867.
- (69) Cebe, P. Introduction to Scattering from Polymers. In *Scattering from Polymers*; ACS Symposium Series; American Chemical Society, 1999; Vol. 739, pp 2–22.
- (70) Kumaraswamy, G.; Verma, R. K.; Kornfield, J. A.; Yeh, F.; Hsiao, B. S. Shear-Enhanced Crystallization in Isotactic Polypropylene. In-Situ Synchrotron SAXS and WAXD. *Macromolecules* **2004**, *37* (24), 9005–9017.
- (71) Padden, F. J.; Keith, H. D. Mechanism for Lamellar Branching in Isotactic Polypropylene. *J. Appl. Phys.* **1973**, *44* (3), 1217–1223.
- (72) Gedde, U. W.; Hedenqvist, M. S. Morphology of Semicrystalline Polymers. In *Fundamental Polymer Science*; Springer International Publishing: Cham, 2019; pp 251–326.
- (73) Balzano, L.; Rastogi, S.; Peters, G. W. M. Flow Induced Crystallization in Isotactic Polypropylene–1,3:2,4-Bis(3,4-Dimethylbenzylidene)Sorbitol Blends: Implications on Morphology of Shear and Phase Separation. *Macromolecules* **2008**, *41* (2), 399–408.
- (74) Somani, R. H.; Hsiao, B. S.; Nogales, A.; Fruitwala, H.; Srinivas, S.; Tsou, A. H. Structure Development during Shear Flow Induced Crystallization of I-PP: In Situ Wide-Angle X-Ray Diffraction Study. *Macromolecules* **2001**, *34* (17), 5902–5909.
- (75) Song, S.; Jiang, J.; Nikbin, E.; Y. Howe, J.; Manners, I.; A. Winnik, M. The Role of Cooling Rate in Crystallization-Driven Block Copolymer Self-Assembly. *Chem. Sci.* **2022**, *13* (2), 396–409.
- (76) Quynn, R. G.; Riley, J. L.; Young, D. A.; Noether, H. D. Density, Crystallinity, and Heptane Insolubility in Isotactic Polypropylene. *J. Appl. Polym. Sci.* **1959**, *2* (5), 166–173.